7 Application of the developed coupling algorithm

Three-dimensional laminar flow around an elastic cylinder

The implicit coupling strategy will be finally applied to a dynamical FSI problem with finite deformations in a complex three-dimensional domain. In the previous sections we gained experience with the two-dimensional laminar flows around rigid and elastic cylinders, in this section the fully three-dimensional flow will be investigated.

Referring to [51] besides the Reynolds number there are additional influencing parameters for these flows. The fluid behaviour depends on the aspect ratio (the ratio between the diameter and the length of the cylinder), the wall blockage (the distance between the channel walls and the cylinder), turbulence and other parameters. If the cylinder is elastic, then the flow is also affected by the cylinder oscillations and deformations. In certain cases some of these influencing parameters may dominate the Reynolds number and may become governing parameters.

Recently, the three-dimensional flows around infinite rigid cylinders and for very big aspect ratios have been studied experimentally and numerically in [51], [28]. However, if the aspect ratio of the cylinder is smaller than 10, there are very few investigations. Some studies for aspect ratio 4.1:1 can be found in [39], where the flow around a rigid fixed cylinder is studied for Reynolds numbers Re = 20 and Re = 100. Contrarily to the two-dimensional flow around a rigid cylinder with Re = 100, the simulations in this benchmark show that the three-dimensional flow with Re = 100 tends to become almost stationary. This is caused by the channel walls on the top and the bottom of the cylinder that have a stabilising effect on the flow.

7.1 Problem formulation

In order to use the experience of the benchmark computations in [39], the same geometry is chosen. The problem description is depicted in Figure 7.1. The cylinder has diameter d = 0.1 m and length H = 4.1d. Its ends are mounted on the top and the bottom walls of a channel with a square cross-section. The cylinder is placed at distance 5d from the inlet and 20d from the outlet, non-symmetrically to the other two channel walls.

As in [39], the fluid density is ρ_{fluid} = 1.0 kg/m^3 and the kinematic viscosity is 10^{-3} m^2/s. However, to get a non-steady flow, the fluid bulk velocity is chosen v_0 = 1.5 m/s. Hence, the corresponding Reynolds number is Re = 150. Nevertheless, the flow is still laminar [51].

At the inlet (at x = 0) a parabolic velocity profile constant in time is applied given by:

$$v_1(0, y, z) = 36 v_0 yz(H - y)(H - z)/H^4 \ , \quad v_2 = 0 \ , \quad v_3 = 0 \tag{7.1}$$

On the other hand the cylinder is assumed to have thin walls with thickness d/25, i.e. 0.004 m. It is made of an elastic isotropic material with Young modulus E= 20 kN/m^2,

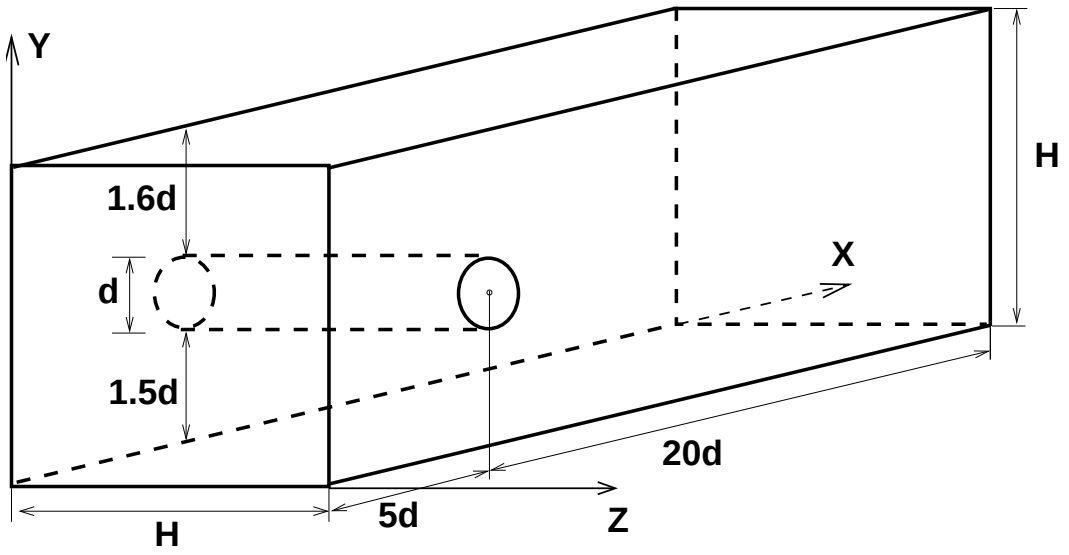

Figure 7.1: Flow around cylinder in a square channel - geometry description

Poisson ratio $\nu = 0.4$ and density $\rho_{struc} = 800$ kg/m^3. The pressure at the inlet is set to coincide to the pressure inside the cylinder. In this way the effects of the external forces on the cylinder walls are reduced and the cylinder deformation will be mainly due to the fluid dynamic forces.

The interaction between the fluid and the elastic cylinder will be investigated. In the beginning of the simulation the flow is taken to be the developed periodic flow around a rigid fixed cylinder.

7.2 Fluid dynamics problem

To obtain the desired initial conditions for the fluid-structure interaction problem, firstly, the laminar flow around the rigid cylinder has to be received. It turned out that the fluid dynamics part itself is a rather complex problem to solve. To apply the solver FASTEST-3D, the fluid domain has to be discretised into a finite-volume block-structured grid. A coarse grid with 24950 control volumes (CVs) is generated at first. It consists of three blocks, each with 10x15x25, 8x46x25 and 30x16x25 CVs. For convenience it will be denoted Grid 1 and is shown in Figure 7.2.

To investigate the effects of the spatial discretisation, two grids Grid 2 and Grid 3 are created through consequently refining Grid 1. They have 199 600 CVs and 1 596 800 CVs, respectively.

Three time-steps are selected for time-discretisation: $\Delta t_1 = 0.005$ s, $\Delta t_2 = 0.0025$ s and $\Delta t_3 = 0.00125$ s.

To obtain high spatial and temporal accuracy the CDS is applied to the spatial derivatives, while the Crank-Nicolson scheme is used for time-stepping. For computational

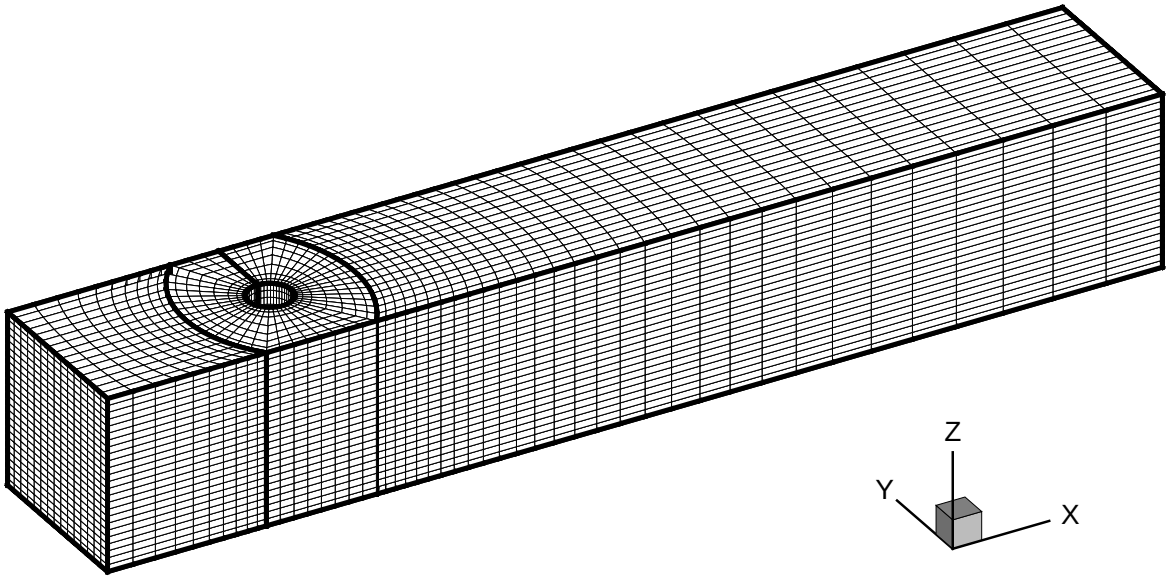

Figure 7.2: Fluid domain discretisation - Grid 1

acceleration a two-level multigrid method is performed to find the solution at every time-step for Grid 2 and a three-level multigrid method is used on Grid 3.

As it was already pointed out in section 6.2 the flow is characterised by the drag and the lift coefficients on the cylinder walls. In the present three-dimensional computations, additionally, the z-component of the fluid dynamic force will be evaluated. The corresponding dimensionless coefficient is denoted C_Z. Hence, in the current notations the three coefficients are defined by

$$C_D = \frac{F_x}{\frac{1}{2}\rho_{fluid} v_0^2 \; dH} \; , \qquad C_L = \frac{F_y}{\frac{1}{2}\rho_{fluid} v_0^2 \; dH} \; , \qquad C_Z = \frac{F_z}{\frac{1}{2}\rho_{fluid} v_0^2 \; dH} \; , \tag{7.2}$$

where F_x, F_y and F_z respectively represent the x-, y- and z- components of the resultant fluid dynamic force exerted on the cylinder.

The drag and lift coefficients obtained on Grid 1 and Grid 2 for the three time-steps are presented in Figures 7.3 and 7.4, respectively.

Though on Grid 1 a periodic state is achieved, it can be seen that on Grid 2 the coefficients oscillate chaotically regardless of the time-step size.

To find the effect of the spatial discretisation along the cylinder, i.e. along the z-axis, one additional grid - Grid 4 is considered. It is obtained from Grid 2 with doubling the number of the grid-points in z-direction and has 399200 CV. The results on Grid 4 are similar to those on Grid 2.

The periodic solution of the fluid problem is obtained for Grid 3 (1 596 800 CV). The received drag and lift coefficients for time-step Δt_2=0.0025s are presented in Figure 7.5. They are compared to the results for Grid 5 (702 592 CV), that is received from Grid 3 with reducing the control volumes number along the cylinder to 44 CVs. A three-level multigrid has also been used on Grid 5.

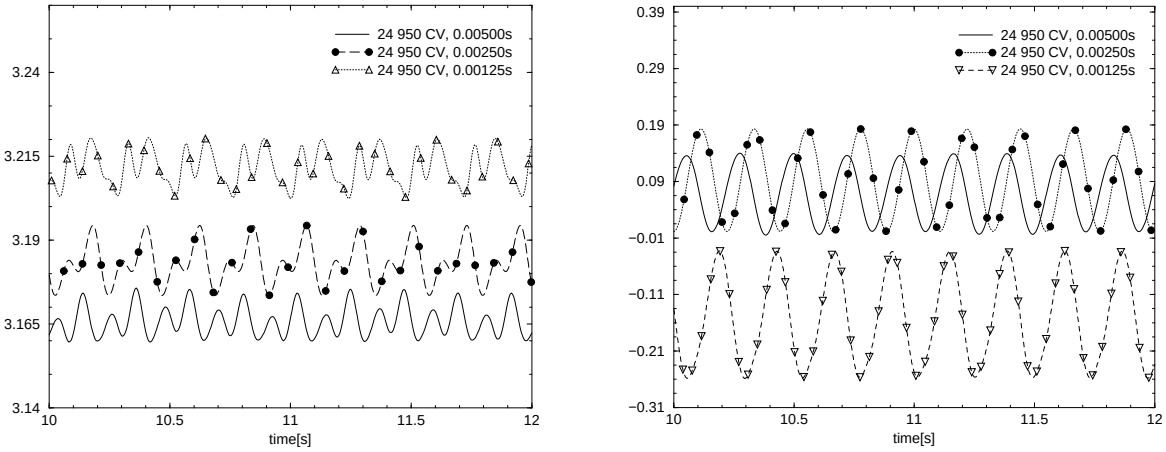

(a) Drag coefficient

(b) Lift coefficient

Figure 7.3: Grid 1 (24 950 CV), different time-steps: Coefficients time history

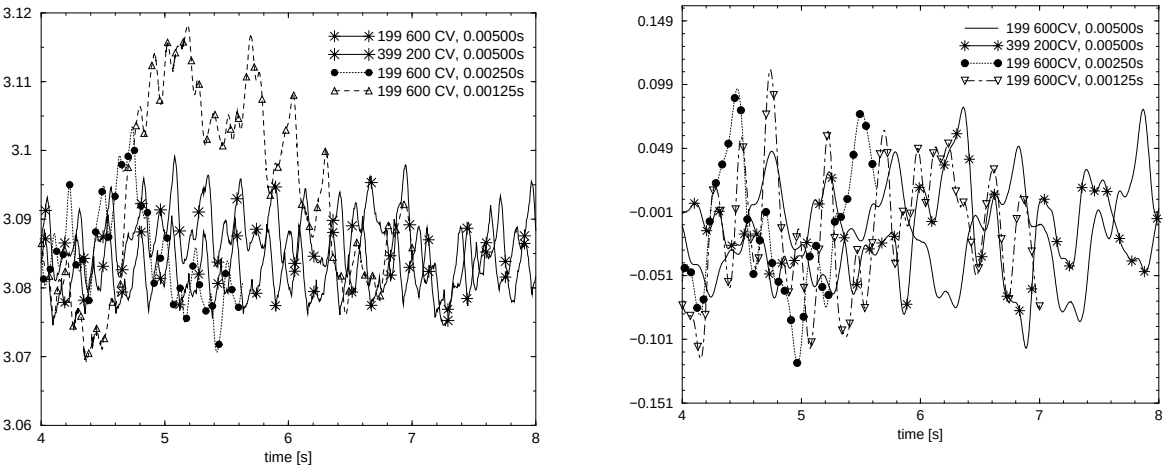

(a) Drag coefficient

(b) Lift coefficient

Figure 7.4: Grid 2 (199 600 CV), different time-steps and Grid 4 (399 200 CV), Δt_1=0.005s: Coefficients time history

It can be observed that the results for C_L on Grid 3 and Grid 5 are in a good agreement. On the other hand C_D is influenced by the spatial discretisation along the cylinder. However, the coefficients are totally different from the solutions for Grid 1, Grid 2 and Grid 4. Therefore, the spatial resolution of Grid 1, Grid 2 and Grid 4 is not enough. It leads to non-physical oscillations of the CDS employed for the spatial discretisation.

On the coarser grids the calculations receive no significant effects in the third, z-direction, where the coefficient C_Z is approximately zero. However, the higher spatial resolutions of Grid 3 and Grid 5 show that C_Z is also periodically oscillating. Its time history is given in Figure 7.6.

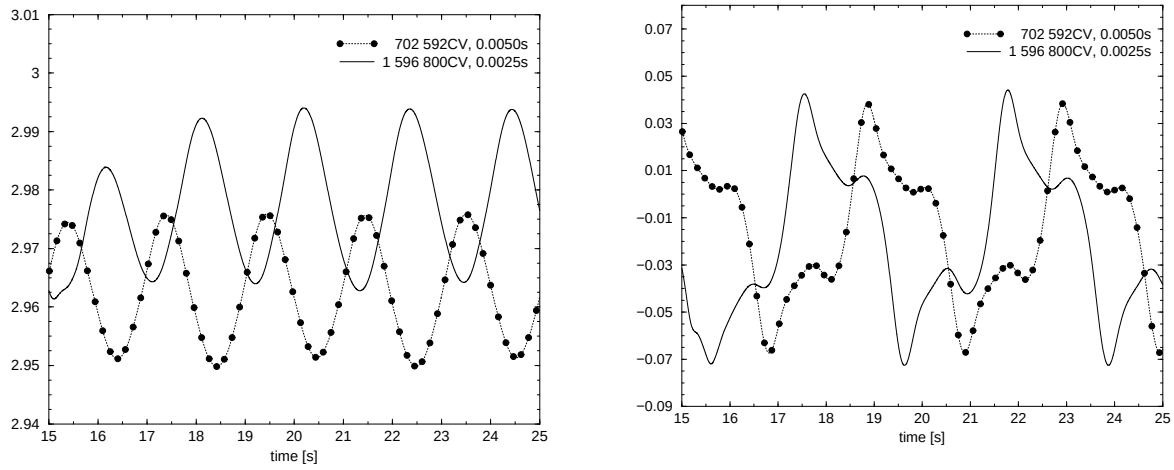

(a) Drag coefficient

(b) Lift coefficient

Figure 7.5: Grid 3 (1 596 800 CV), Δt_2=0.0025s and Grid 5 (702 592 CV), Δt_1=0.005s: Coefficients time history

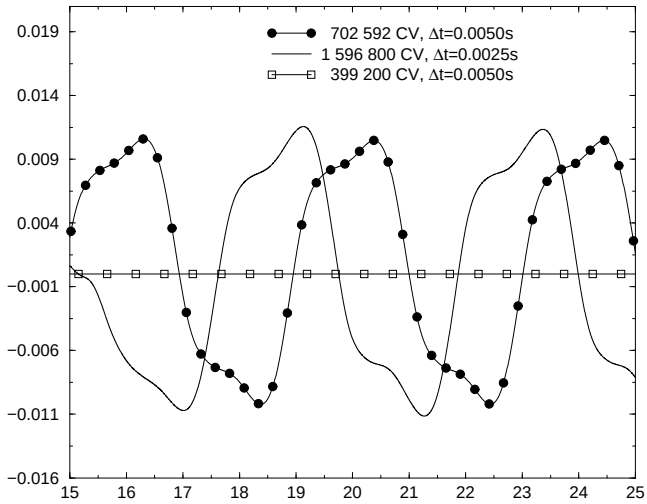

Figure 7.6: Time history of the coefficient C_Z: Grid 3 (1 596 800 CV), Δt_2=0.0025s, Grid 5 (702 592 CV), Δt_1=0.005s and Grid 4 (399 200 CV), Δt_1=0.005s

The results obtained on Grid 3 at time 31.5 s for time-step Δt_2=0.0025s are presented in Figures 7.7 and 7.8.

In Figure 7.7 the pressure isosurfaces are depicted. Two unsymmetrical areas of low pressure are formed behind the cylinder. On the other hand the inlet flow leads to a high pressure at the front part of the body. Additionally, two districts of a lower pressure appear on the walls of the cylinder. The unsymmetrical wake can also be noticed in the x-component of the fluid velocity presented in Figure 7.8. Here, the x-velocity distribution at different y-planes of the channel are depicted. For better visualisation the z-coordinates are scaled with factor 3. Though at the middle plane

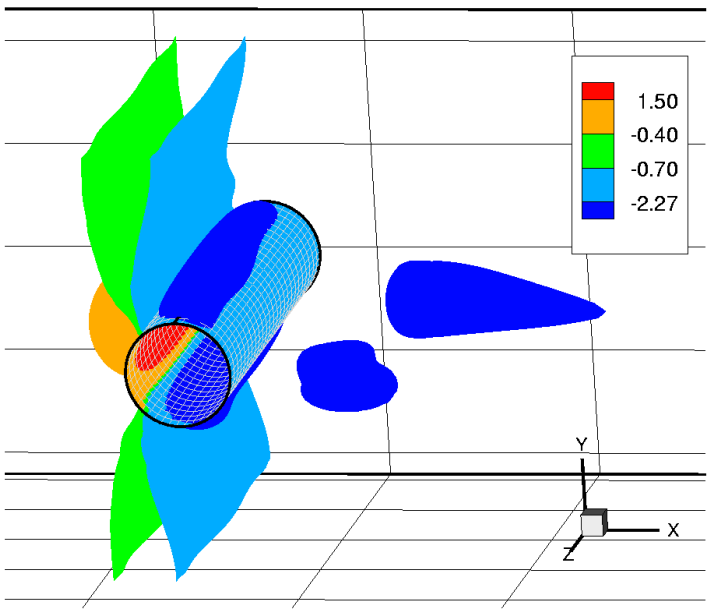

Figure 7.7: Pressure isosurfaces (Grid 3 (1596800 CV), Δt_2=0.0025s)

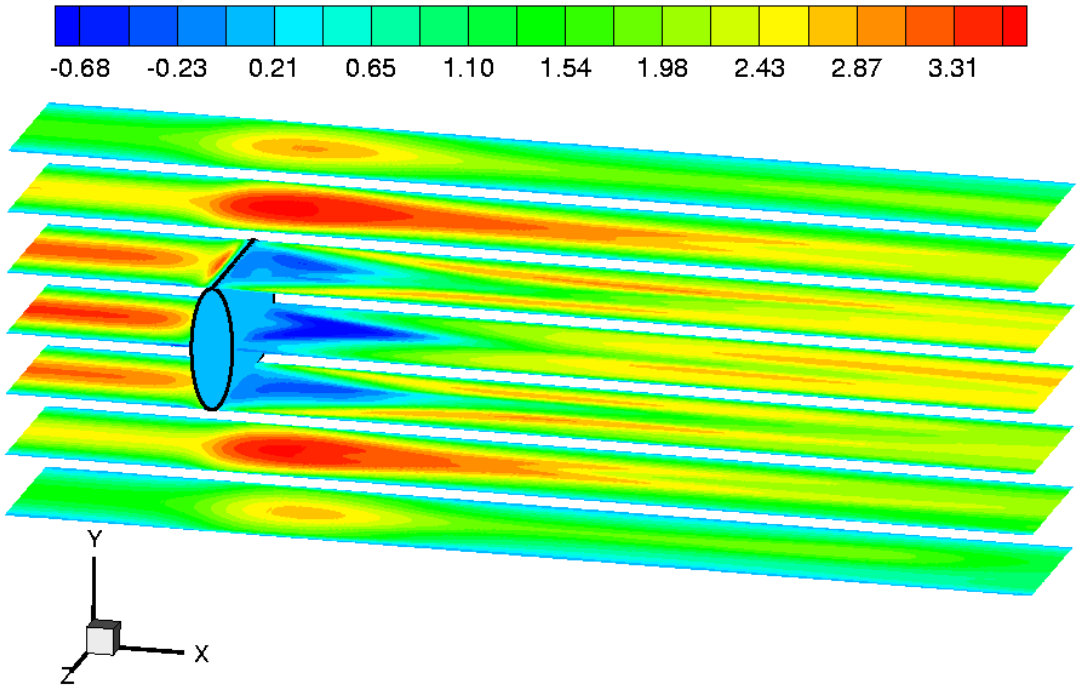

Figure 7.8: x-component of the fluid velocity (Grid 3 (1596800 CV), Δt_2=0.0025s)

y = H/2 the velocity is almost symmetric, in the neighbour planes non-symmetric effects can be noticed. Hence, the flow is three-dimensional and unsteady.

7.3 Fluid-structure interaction

The investigation of the three-dimensional flow around a rigid cylinder shows that a fine spatial resolution is required for obtaining the correct solution. Therefore, to simulate the FSI when the cylinder is elastic, only the finest grid, Grid 3, will be used. The time-step $\Delta t_2 = 0.0025$ s is chosen for time discretisation. For initial flow conditions the periodic flow presented in section 7.2 is taken. Since finite deformations of the elastic cylinder will be considered, the implicit coupling method is applied. Again, for reducing the computational time a three-level multigrid is used so that 2 V-cycles per predictor-corrector iteration are allowed.

Structural domain discretisation

To solve the structural part of the FSI problem, a suitable discretisation of the cylinder walls is required. For this purpose the 4-nodes shell elements are chosen. They have 5 degrees of freedom (3 translations and 2 rotations) and are able to model finite deformations. If the structural nodes exactly coincide to the fluid grid-points on the cylinder, then their number would be 17600. Hence, tremendous computational time would be required for solving the structural part at every prediction-correction. On the other hand the use of shape functions by the finite elements allows coarse grids to be considered. Therefore, the approach proposed in section 5.1 for a spatial discretisation of the structure is not appropriate.

To reduce the number of nodes, the structural grid is chosen to coincide to the coarsest fluid grid (Grid 1) on the cylinder. Hence, 1100 structural nodes are used. Both spatial discretisations of the elastic walls are depicted in Figure 7.9.

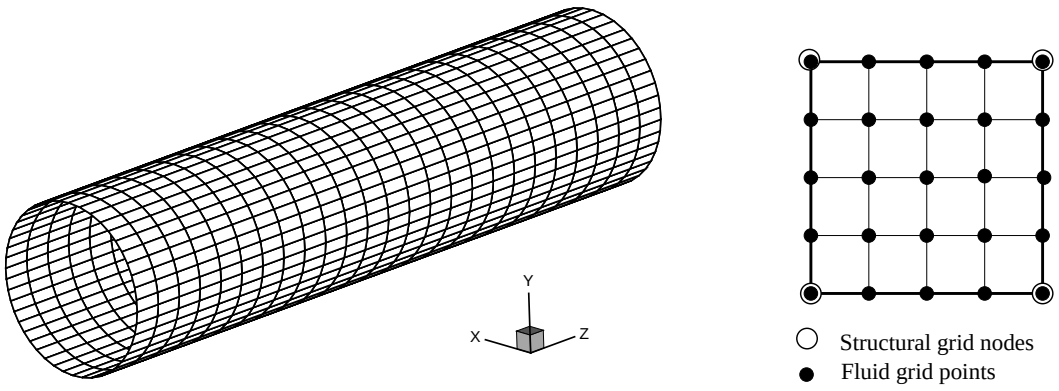

(a) Structural grid (b) Grids - a zoom

Figure 7.9: Cylinder spatial discretisations

The advantage of this grid choice is that the fluid force at a structure node can be naturally found by summing the forces at the fluid CV centers shown in Figure 7.10. In this way the total force acting on the fluid boundary are the same as the total force acting on the structure and an energy conservation on the interface is assured.

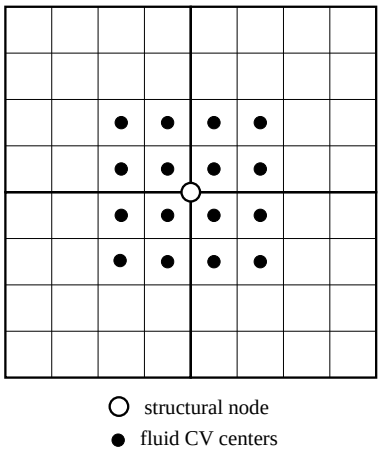

Figure 7.10: Cylinder wall: Fluid dynamic force projection

Additionally, since the structural nodes coincide to some of the fluid grid-points, no approximation of their displacements is needed. The displacements at the rest of the fluid points may be easily found using a linear interpolation.

Numerical simulation

Finally, the FSI problem described in section 7.1 will be investigated within a time interval of 11.5 s.

In Figure 7.7 it can be observed that in the beginning the highest pressure is at the front part of the cylinder. Therefore, here, the biggest deformation is expected. Additionally, the lower pressure on the other two sides of the cylinder will lead to flattening of the cylinder walls. The deformed cylinder at the end of the simulation (at time 11.25s) is presented in Figure 7.11.

To study the dynamic variation of the displacements, four points placed exactly in the middle of the cylinder are specially monitored. Their positions can be seen in Figure 7.12. The time history of the displacements of these points are shown in Figure 7.13.

In the beginning of the simulation all displacements reach their absolute maxima. Then they start oscillating around some average values. Since the points are at equal distances to the ends of the cylinder, their z-displacements are nearly zero.

Obviously, the biggest displacement is the x-displacement at the front point 1. It is fluctuating around 0.016m. Due to the different wall blockage factors of the cylinder, the y-displacement of the point 1 is oscillating around -0.002 m, i.e. around a non-zero

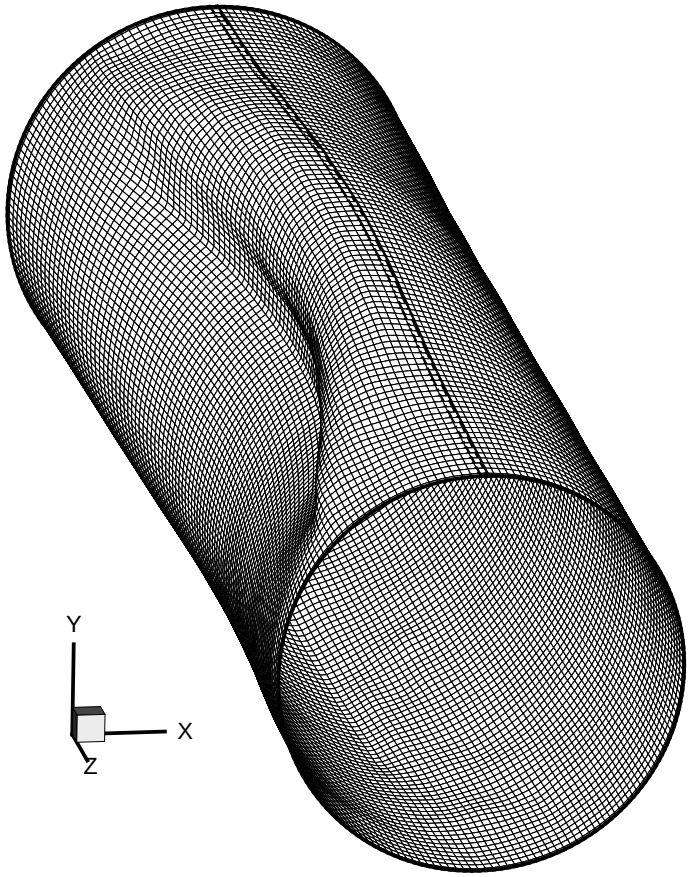

Figure 7.11: FSI: Deformed cylinder

number. Therefore, the cylinder walls are not only flattened but also twisted by the fluid dynamic forces. On the other hand the smallest displacements are at the back point 2. Its x-displacement is the largest and has average value -0.003 m.

The effects of the non-symmetrical position of the cylinder are also observed in the deformations at the points 3 and 4. Their y-displacements are the biggest and are fluctuating around -0.007 m and 0.006 m, respectively. On the other hand the average x-displacement of point 3 is rather small, i.e. it is 0.0003 m, while the same of point 4 is 0.0023 m.

The coefficients C_D, C_L and C_Z also change their amplitudes and frequencies. In Figure 7.14 their time histories are presented. For comparison the results without considering FSI are shown. The FSI is taken into account from time 0 s.

Due to the deformation the cylinder area exposed to the flow increases. This leads to a bigger drag coefficient and to a bigger absolute value of the average lift coefficient. Additionally, the periods of oscillations decrease. In Figure 7.14(a) it can be noticed that the coefficient C_D tends to a periodic state. The coefficients C_L and C_Z also oscillate, however, periodic states are not yet obtained. The reason is that the flow pattern is more complex than the one for a rigid cylinder. Therefore, a longer simulation

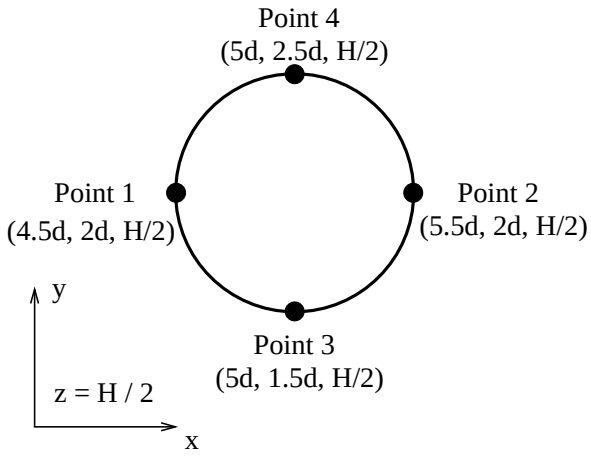

Figure 7.12: Monitored points

time (more than 11.5 s) is needed to receive the periodic FSI state. Additionally, a finer spatial discretisation may be required by the FSI problem.

The pressure isosurfaces are presented in Figure 7.15. The highest pressure remains at the front part of the body. However, the pressure behind the cylinder has a much more complex pattern than the one for a rigid cylinder. The comparison between the results in Figures 7.7 and 7.15 shows that when the fluid-structure interaction is considered the pressure distribution changes. Moreover, stronger non-symmetric three-dimensional effects are observed.

Accordingly, the x-component of the fluid velocity is also different. It is depicted in Figure 7.16, where the z-coordinates are scaled with factor 3 for a better visualisation.

Due to the very small time-step 0.0025s, only two predictor-corrector iterations have been enough for finding the fluid-structure equilibrium at every time-step.

The numerical simulation shows that the created implicit coupling algorithm can be successfully applied to dynamical FSI problems with finite deformations in three-dimensional domains.

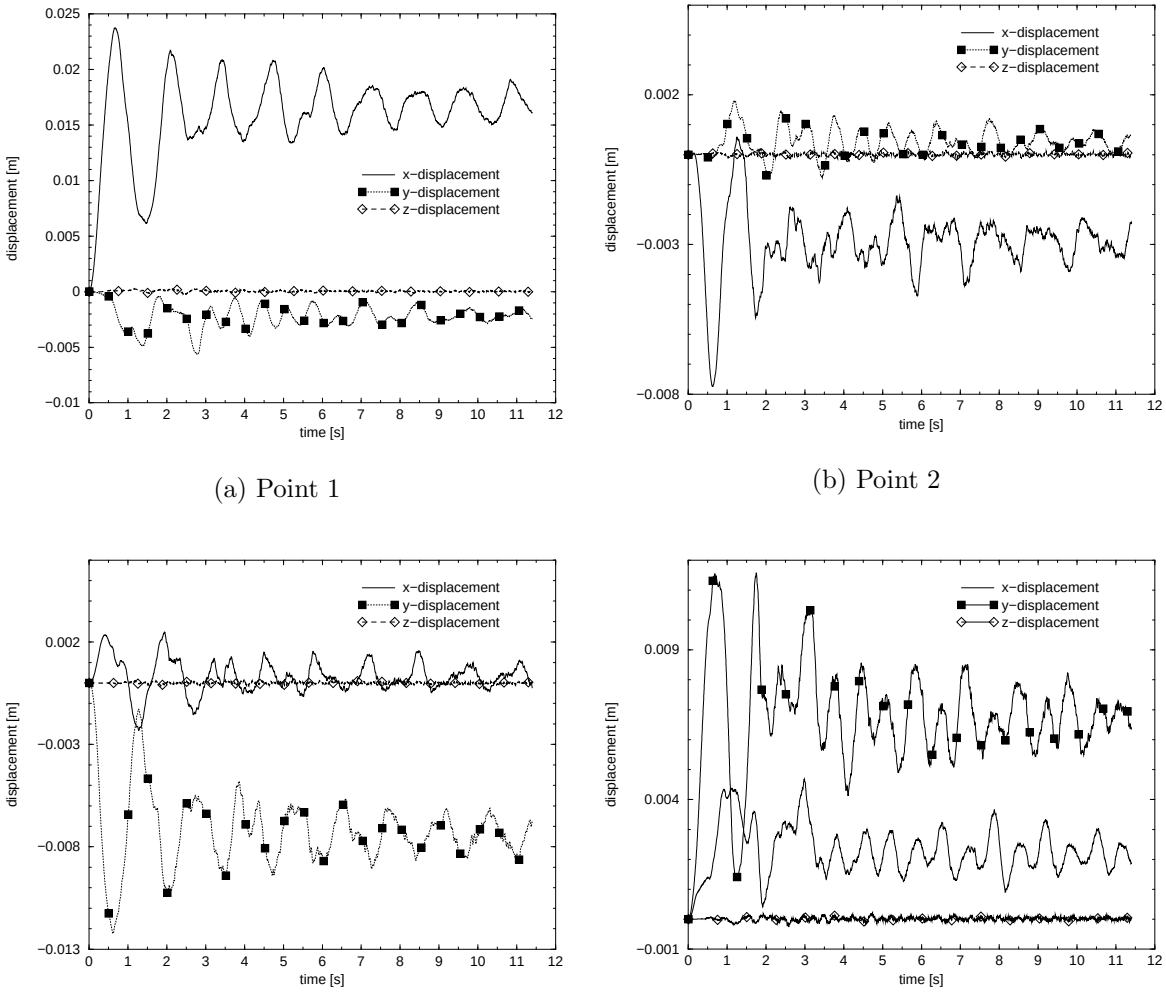

(a) Point 1

(b) Point 2

(c) Point 3

(d) Point 4

Figure 7.13: FSI: Displacements time history

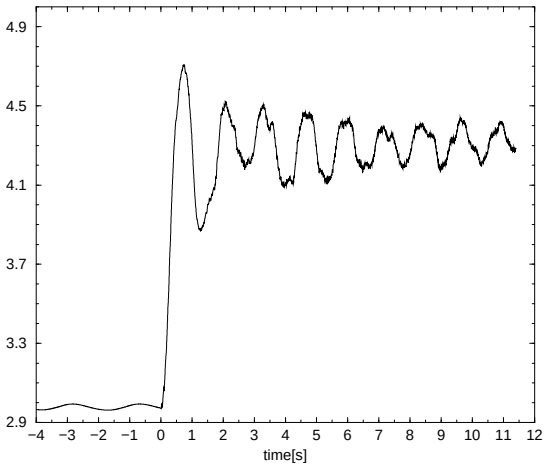

(a) Drag coefficient C_D

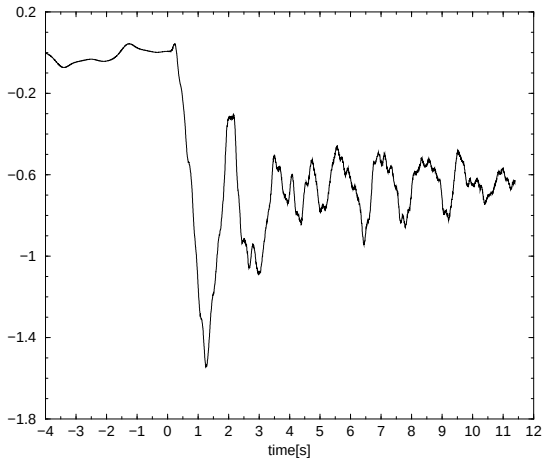

(b) Lift coefficient C_L

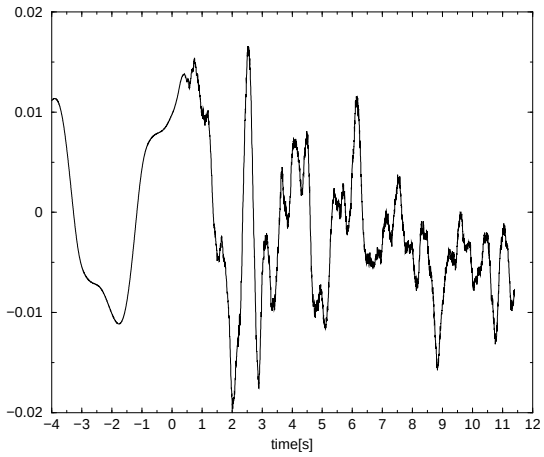

(c) C_Z coefficient

Figure 7.14: FSI: time history of the coefficients

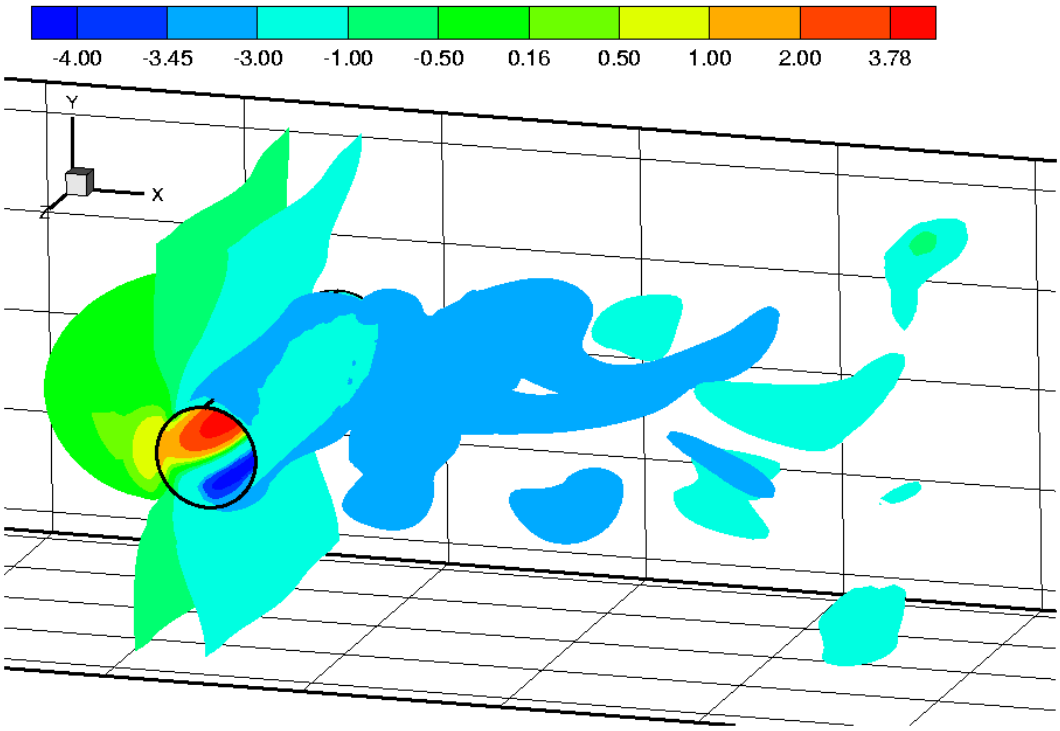

Figure 7.15: FSI: Pressure isosurfaces

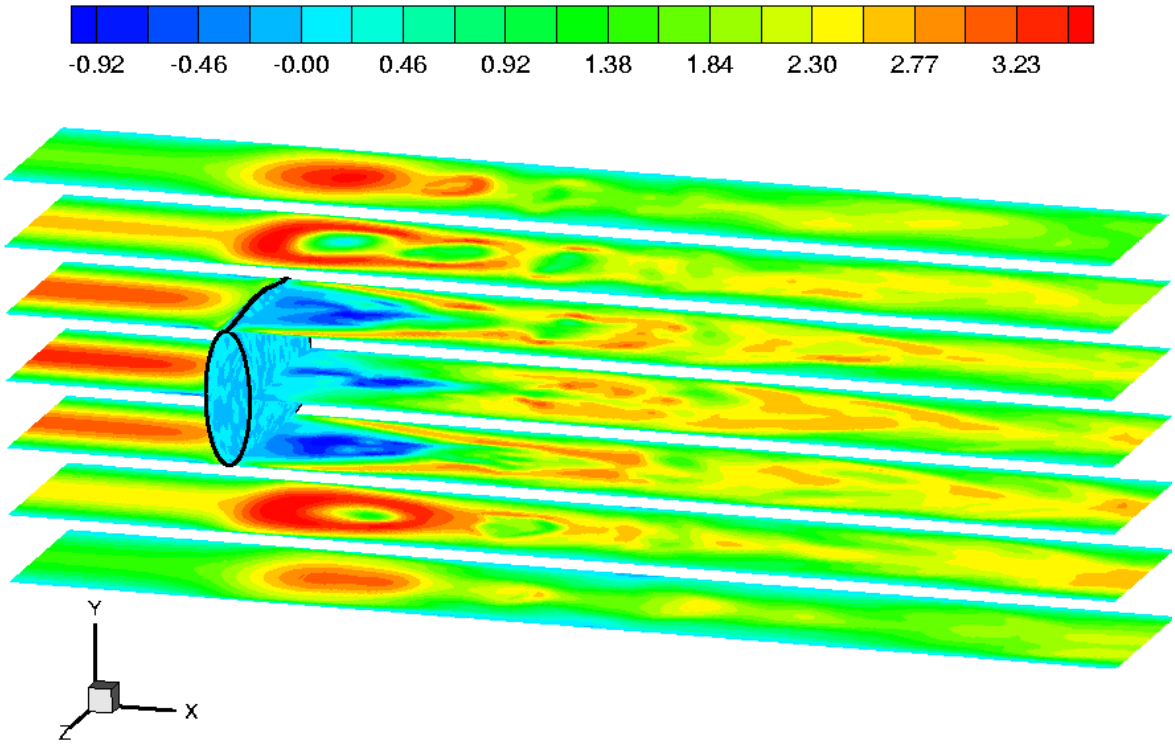

Figure 7.16: FSI: x-component of the fluid velocity

8 Conclusion and Outlook

In the present work an explicit and an implicit loose coupling method for the numerical simulation of three-dimensional fluid-structure interaction (FSI) problems have been developed. For this purpose the finite volume code FASTEST-3D has been applied to the fluid dynamic subproblem and the finite element program FEAP has been used for the structural dynamic subtask. These solvers have been coupled using loose coupling approach in which the fluid and the structural parts are solved in a staggered manner. For modelling the FSI, the pressure and shear forces of the fluid flow are projected into the structural nodes and applied as boundary conditions for the structure. To account for the fluid domain movement caused by the structural deformation, the fluid solver has been modified so that it can also treat problems described in Eulerian-Lagrangian (moving) coordinates. The fluid grid is updated to match the new domain boundaries using a linear interpolation. Hence, the space conservation law is added to the Navier-Stokes equations and a total mass conservation has been assured. Currently, moving grids have been implemented into the fluid code for the first-order implicit Euler and the second-order Crank-Nicolson time-stepping schemes. In the explicit coupling method the information between the solvers is exchanged only once per time-step. On the other hand the implicit coupling strategy is based on a predictor-corrector scheme for finding the fluid-structure equilibrium at every time-step.

It turned out that the explicit coupling algorithm can be applied to problems with small deformations. It was used to simulate the laminar flow in an elastic pipe with two periodic pinching forces and to find the steady state of a laminar flow in a 90^0 T-junction of elastic pipes. However, this method is not suitable for dynamical problems with finite deformations because of its restriction on the time-step size. For these FSI problems the implicit coupling strategy is advantageous. The created predictor-corrector scheme has been successfully applied to both steady and dynamic FSI tasks with finite deformations. The dynamical FSI of a laminar flow around an elastic cylinder for $\mathrm{Re} = 20$ and $\mathrm{Re} = 100$ has been studied.

The numerical investigation of the implicit coupling method showed that it has very good convergence properties. It can use time-steps that are bigger than the time-steps required by the explicit algorithm. However, when the time-step is increased, the structural displacements and respectively, the fluid domain deformation become bigger. Consequently, the number of the predictor-corrector iterations necessary for finding the fluid-structure equilibrium also increases. On the other hand, if the time-step is small enough then only one prediction-correction is enough and the implicit method coincides to the explicit one.

Finally, the three-dimensional unsteady flow around an elastic cylinder mounted in a square channel was successfully modelled. In this way the application of the created implicit coupling method to complex three-dimensional dynamic FSI problems has been demonstrated. Further experimental and theoretical investigations are required for the validation of the proposed coupling strategies.

In the current simulations only deformations that do not change the fluid grid topology have been considered. Additional modifications of the fluid solver are needed to model

FSI problems in which the grid topology may change. Such problems may be treated for example through combining moving grids with clicking and deforming meshes.

Though in the present research, the FSI through the temperature field has been neglected, the developed coupling methods can be further extended to solve fully coupled FSI problems, i.e. with interaction not only through the fluid forces and deformations, but also through the temperature.

The created coupling strategies have successfully modelled the considered test examples. Therefore, they can be further applied to solve practical FSI problems. Moreover, depending on the generality of the used fluid and structural codes, the developed coupling methods are also able to simulate various FSI tasks.

References

[1] N. Galanis B. Benhamou and A. Laneville. Transient effects of orthogonal pipe oscillations on laminar developing incompressible flow. *International Journal for Numerical Methods in Fluids*, 34:561–584, 2001.

[2] K.-C. Park C. A. Felippa and C. Farhat. Partitioned analysis of coupled systems. *Computational Mechanics, Barcelona, Spain*, 1998.

[3] M. Lesoinne C. Farhat and P. LeTallec. Load and motion transfer algorithms for fluid/structure interaction problems with non-matching discrete interfaces: Momentum and energy conservation, optimal discretization and application to aeroelasticity. *Computer Methods in Applied Mechanics and Engineering*, 157:95–114, 1998.

[4] J. R. Cebral. *Loose coupling algorithms for Fluid Structure Interaction*. PhD thesis, Institute for Computational Science and Informatics, George Mason University, 1996.

[5] J. R. Cebral and R. Löhner. Conservative load projection and tracking for fluid–structure problems. *AIAA Journal*, 35:4:687–692, 1997.

[6] A. Combescure and N. Greffet. Coupled fluid–structure simulation: non-linear instability problems under steady viscous flows. *Proceedings of ECCM'99*, 1999.

[7] C. Cossu and L. Morino. On the instability of a spring-mounted circular cylinder in a viscous flow at low reynolds numbers. *Journal of Fluids and Structures*, 14:183–196, 2000.

[8] I. Demirdžić and M. Perić. Space conservation law in finite volume calculations of fluid flow. *International Journal for Numerical Methods in Fluids*, 8:1037–1050, 1988.

[9] I. Demirdžić and M. Perić. Finite volume method for prediction of fluid flow in arbitrarily shaped domains with moving boundaries. *International Journal for Numerical Methods in Fluids*, 10:771–790, 1990.

[10] J. Donea. Arbitrary lagrangian-eulerian finite element methods. In *Computational Methods for Transient Analysis*, volume 1 of *Computational Methods in Mechanics*, pages 473–503. Elsevier Science Publishers B. V., 1983.

[11] C. Farhat and M. Lesoinne. Geometric consevation laws for flow problems with moving boundaries and deformable meshes, and their impact on aeroelastic computations. *Computer Methods in Applied Mechanics and Engineering*, 134:71–90, 2000.

[12] C. Farhat and M. Lesoinne. Two efficient staggered algorithms for the serial and parallel solution of three-dimensional nonlinear transient aeroelastic problems. *Computer Methods in Applied Mechanics and Engineering*, 182:499–515, 2000.

[13] F. Felker. Direct solution of two-dimensional navier-stokes equations for static aeroelasticity problems. *AIAA Journal*, 31:148–153, 1993.

[14] H. Ferziger and M. Perić. *Computational Methods for Fluid Dynamics*. Springer, Berlin, second edition, 1997.

[15] H. Guillard and C. Farhat. On the significance of the geometric conservation law for flow computations on moving meshes. *Computer Methods in Applied Mechanics and Engineering*, 190:1467–1482, 2000.

[16] W. Hackbusch. *Multi-Grid Methods and Applications*. Springer, Berlin, 1985.

[17] T. Hughes. Analysis of transient algorithms with particular reference to stability behaviour. *Computational Methods for Transient Analysis, in Computational Methods in Mechanics*, 1:67–153, 1983.

[18] INVENT Computing GmbH. *FASTEST - parallel multigrid solver for flows in complex geometries*, 1994.

[19] J. S. Jensen. Fluid transport due to nonlinear fluid–structure interaction. *Journal of Fluids and Structures*, 11:327–344, 1997.

[20] P. Kjellgren and J. Hyvärinen. An arbitrary lagrangian-eulerian finite element method. *Computational Mechanics*, 21:81–90, 1998.

[21] K. Kounanis and D. S. Mathioulakis. Experimental flow study within a self oscillating collapsible tube. *Journal of Fluids and Structures*, 13:61–73, 1999.

[22] M. A. Langthjem and Y. Sugiyama. Vibration and stability analysis of cantilevered two-pipe systems conveying different fluids. *Journal of Fluids and Structures*, 13:251–268, 1999.

[23] R. Redler M. G. Hackenberg, P. Post and B. Steckel. Mpcci, multidisciplinary applications and multigrid. In *Proceedings ECCOMAS 2000*, CIMNE, Barcelona, 2000.

[24] R. K. Kapania M. K. Bhardwaj and G.P. Guruswamy. Computational fluid dynamics/computational structural dynamics interaction methodology for aircraft wings. *AIAA Journal*, 36:12:2179–2186, 1998.

[25] S. Mittal and V. Kumar. Finite element study of vortex-induces cross-flow and in-line oscillations of a circular cylinder at low reynolds numbers. *International Journal for Numerical Methods in Fluids*, 31:1087–1120, 1999.

[26] S. Natarajan and M. R. Mokhtarzadeh-Dehghan. Numerical prediction of a (potential) soft acting peristaltic blood pump. *International Journal for Numerical Methods in Fluids*, 32:711–724, 2000.

[27] N. Newmark. A method of computation for structural dynamics. *Journal of the Engineering Mechanics Division*, 85:67–94, 1959.

[28] C. Norberg. An experimental investigation of the flow around a circular cylinder: influence of aspect ratio. *Journal of Fluid Mechanics*, 258:287–316, 1994.

[29] L. G. Olson and D. Jaminson. Application of a general purpose finite element method to elastic pipes conveying fluid. *Journal of Fluids and Structures*, 11:207–222, 1997.

[30] M. P. Paidoussis. *Fluid-Structure Interactions*, volume 1. Academic Press, San Diego, 1998.

[31] K. C. Park and C. A. Felippa. Partitioned analysis of coupled systems. *Computational Methods for Transient Analysis in Computational Methods in Mechanics*, 1:157–218, 1983.

[32] S.V. Patankar and D.B. Spalding. A calculation procedure for heat, mass and momentum transfer in three dimensional parabolic flows. *Journal Heat Mass Transfer*, 15:1787–1806, 1972.

[33] T. J. Pedley and K. D. Stephanoff. Flow along a channel with a time-dependent indentation in one wall: the generation of vorticity waves. *Journal of Fluid Mechanics*, 160:337–367, 1985.

[34] M. E. Ralph and T. J. Pedley. Flow in a channel with a moving indentation. *Journal of Fluid Mechanics*, 190:87–112, 1988.

[35] M. E. Ralph and T. J. Pedley. Viscous and inviscid flows in a channel with a moving indentation. *Journal of Fluid Mechanics*, 209:543–566, 1989.

[36] C.M. Rhie and W.L. Chow. Numerical study of the turbulent flow past an airfoil with trailing edge separation. *AIAA Journal*, 21:1525–1532, 1983.

[37] C. Cebral S. Piperno and B. Larrouturou. Partitioned procedures for the transient solution of coupled aeroelastic problems. part 1: Model problem, theory and two-dimensional application. *Journal of Computer Methods in Applied Mechanics and Engineering*, 124:79–112, 1995.

[38] M. Schäfer. *Numerik im Maschinenbau*. Springer, Berlin, 1999.

[39] M. Schäfer and S. Turek. Benchmark computations of laminar flow around cylinder. In E.H. Hirschel, editor, *Flow Simulation with High-Performance Computers II*, volume 52 of *Notes on Numerical Fluid Mechanics*, pages 547–566. Vieweg, 1996.

[40] I. Sheridan and J. Carberry. Special brief note on the near-wake topology of an oscillating cylinder. *Journal of Fluids and Structures*, 12:215–220, 1998.

[41] R. Sieber. *Numerische Simulation technisher Strömungen mit Fluid-Struktur-Kopplung*. PhD thesis, Department of Numerical Methods in Mechanical Engineering, Technische Universität Darmstadt, 2002.

[42] J. Steindorf and H. G. Matthies. Numerical efficiency of different partitioned methods for fluid-structure interaction. In *ZAMM 80 (S2)*, pages 557–558, 2000.

[43] H. L. Stone. Iterative solution of implicit approximations of multidimensional partial differential equations. *SIAM Journal of Numerical Analysis*, 5:530–558, 1968.

[44] C. B. Jenssen T. Kvamsdal, J. Amundsen and K. M. Okstad. Numerical methods for fluid–structure interactions of slender structures. *Proceedings of ECCM'99*, 1999.

[45] P. Le Tallec and S. Mani. Conservation laws for fluid-structure interactions. In T. Kvamsdal, editor, *Proceedings of FSI'99*, Trondheim, 1999.

[46] R. L. Taylor. *Feap - A Finite Element Analysis Program. Version 6.3 User Manual*. Technical report, Dep. Civil and Earthquake Engineering, UC Berkeley, 1998.

[47] S. Timoshenko and J. N. Goodier. *Theory of Elasticity*. McGraw-Hill, second edition, 1951.

[48] D. P. Mok W. A. Wall and E. Ramm. Partitioned analysis approach for the transient, coupled response of viscous fluids and flexible structures. In *ECCM'99 - Proc. European Conference on Computational Mechanics*, 1999.

[49] W. A. Wall. *Fluid-Struktur-Interaktion mit stabilisierten Finiten Elementen*. PhD thesis, Institut für Baustatik, Universität Stuttgart, 2000. Bericht Nr. 31.

[50] W. M. Wood. *Practical Time-stepping Schemes*. Oxford University Press, New York, 1990.

[51] M. M. Zdravkovich. *Flow around circular cylinders*, volume 1. Oxford University Press, New York, 1997.

[52] O. C. Zienkiewicz and R. L. Taylor. *The Finite Element Method*, volume 1. McGraw–Hill, London, 4 edition, 1989.

[53] O. C. Zienkiewicz and R. L. Taylor. *The Finite Element Method*, volume 2. McGraw–Hill, London, 4 edition, 1989.

CURRICULUM VITAE

Name:	Galina Hristova Sieber (maiden name: Vatkova)
Date of Birth:	18. December 1973
Place of Birth:	Pleven, Bulgaria (BG)
Nationality:	Bulgarian
Marital status:	married since November 2000

1980 - 1987	Basic School, Pleven (BG)
1987 - 1990	Mathematical High School "Geo Milev", Pleven (BG) June 1990 graduated one year prior to the expected graduation 1990 classified at the National Olympiad in Mathematics 1990, accepted in all Bulgarian Universities with an entrance exam in mathematics
1990 - 1995	Student in the Faculty of Mathematics and Informatics at Sofia University "St. Kliment Ohridski", Sofia (BG) 1990 - 1993 basic study in mathematics 1993 - 1995 specialisation in the Department of Numerical Methods and Algorithms Master's thesis: "Correctness and Singularities of the Interpolation with Shifted Box-Splines" minor: teacher of mathematics and informatics
1995 - 1998	Mathematician at Laboratory "Geospace Hydrodynamics", Institute of Mechanics, Bulgarian Academy of Sciences, Sofia (BG)
1998 - 2001	PhD student in DFG Graduate College "Modelling and Numerical Description of Technical Flows" at the Department of Numerical Methods in Mechanical Engineering, Darmstadt University of Technology